Food Packaging and Shelf Life 43 (2024) 101280

Contents lists available at ScienceDirect

Food Packaging and Shelf Life

journal homepage: www.elsevier.com/locate/fpsl

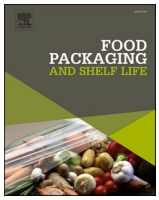

ZnO and Fe_2TiO_5 nanoparticles obtained by green synthesis as active components of alginate food packaging films

Zorka Z. Vasiljevic [a], Jovana Vunduk [b], Milena P. Dojcinovic [a], Goran Miskovic [c], Nenad B. Tadic [d], Jasmina Vidic [e,*], Maria Vesna Nikolic [a,*]

[a] University of Belgrade – Institute for Multidisciplinary Research, 11030 Belgrade, Serbia
[b] Institute of General and Physical Chemistry, 11158 Belgrade, Serbia
[c] Silicon Austria Labs GmbH, High Tech Campus Villach, A-9524 Villach, Austria
[d] University of Belgrade, Faculty of Physics, 11000 Belgrade, Serbia
[e] Université Paris-Saclay, Micalis Institute, INRAE, AgroParisTech, 78350 Jouy-en-Josas, France

ARTICLE INFO

Keywords:
ZnO nanoparticles
Fe_2TiO_5 nanoparticles
Green synthesis
Alginate film
Composite film

ABSTRACT

The aim of this study was to develop an active alginate packaging film incorporating antioxidant Fe_2TiO_5 and antibacterial ZnO nanoparticles, obtained by green synthesis utilizing citrus peel waste. The average particle size was estimated as 10 nm for ZnO and 50 nm for Fe_2TiO_5. Films were prepared using 2.33% (w/v) sodium alginate with 0.11% (w/v) Fe_2TiO_5 and/or ZnO nanoparticles. The inclusion of nanoparticles resulted in a noticeable colour difference, reduced the transparency, increased UV light protection and improved thermal stability of the film. The dry matter content of the films was around 83%. Film solubility in distilled water was low (< 8%) mainly reflecting crosslinking of the alginate polymer and Ca^{2+}-ions. The lowest swelling degree was obtained for the ZnO/Fe_2TiO_5 –alginate film (178%). The efficiency of these packaging films was demonstrated through preservation of strawberry freshness. Alginate packaging film with a mixture of metal oxide nanoparticles can facilitate food safety and increase food shelf life.

1. Introduction

Development of advanced food packaging materials modified by nanotechnology, nanomaterials and nanoparticles has resulted in longer food shelf life and smart food packaging functions, tracing the path towards more sustainable packaging solutions (Ahmad et al., 2023). Food packaging material for the future needs actively to protect the food product, indicate and reduce spoilage, and extend product shelf life. The material should be composed of biodegradable and non-polluting components. Replacement of petrochemical plastic polluting food packaging films with biodegradable alternatives, such as polysaccharides - alginate, chitosan, starch, etc., lipids and proteins is an objective of upcoming packaging solutions. Biodegradable polymer films can be sourced from fruit and vegetable processing by-products, especially as about 45% of fruits and vegetables produced worldwide are presently wasted. Such a green approach would bring about recycling, increased worth, and reduce environmental pollution (Lau, Sabran, & Shafie, 2021; Sani et al., 2023). Sodium alginate, a derivative of alginate, is a non-toxic biodegradable polysaccharide, made up of guluronic and manuronic acid molecules bound by 1 − 4 glycosidic bonds. The US-FDA generally regards this polysaccharide as safe (GRAS) (Teng, An, Chen, Zhang, & Zhao, 2021; Motelica et al., 2021). Sodium alginate is water soluble and can be easily functionalized. Cross-linking with polyvalent cations, such as Ca^{2+}, makes sodium alginate water-resistant and applicable for food packaging films (Omerović et al., 2021; Giz et al., 2020; Omerović et al., 2021). Plasticizers, for instance glycerol, have been added to improve the mechanical properties of alginate packaging films, but both mechanical and barrier properties need to be further enhanced by incorporating nanoparticles, essential oils or plant extracts (Motelica et al., 2021).

The mechanical, thermal and barrier properties of biopolymer packaging films have been advanced by incorporation of metal oxide nanoparticles (Nikolic et al., 2021; Lopusiewicz et al., 2022). Alginate reinforced with metal oxide nanoparticles has been investigated in the form of hydrogels (Sattayapanich, Chaiwat, Boonmarte, Bureekaem, & Sutthasupa, 2022), films (Vizzi, Beltrame, Zanet, Vidic, & Manzano, 2020; Rizzotto et al., 2022; Motelica et al., 2021; Sarvanakumar et al., 2020) and coatings (Parreidt, Müller, & Schmid, 2018; Aziz & Salama,

* Corresponding authors.
E-mail addresses: jasmina.vidic@inrae.fr (J. Vidic), mariavesna@imsi.bg.ac.rs (M.V. Nikolic).

https://doi.org/10.1016/j.fpsl.2024.101280
Received 14 February 2023; Received in revised form 28 March 2024; Accepted 31 March 2024

2021) for active food packaging. The antioxidant, antimicrobial and antifungal functions of biodegradable food packaging films, including alginate, have been improved by incorporation of metal oxide nanoparticles (Omerović et al., 2021).

Zinc-oxide (ZnO) is a semiconducting metal oxide extensively investigated for quite some time. Its broad application field includes food packaging and preservation (Zare et al., 2022). The US FDA considers ZnO nanoparticles (NPs) as GRAS. ZnO NPs displayed good antibacterial activity and have been used as components in food packaging composite materials (Phothisarattana, Wongphan, Promhwad, Promsoru, & Harnkarnujant, 2022; Shankar & Rhim, 2019; Motelica et al., 2021). However, the antibacterial activity of ZnO NPs is due to interactions with bacterial cells. Therefore, besides benefits, there are some risks of utilizing ZnO NPs in food packaging film as NPs may migrate and interact with human cells (Pei et al., 2022; Czyżowska & Barbasz, 2022). Titanium oxide NPs have also been investigated for use in food packaging (Nikolic, Vasiljevic, Auger, & Vidic, 2021; Omerovic et al., 2021; Saravanakumar et al., 2020). However, there are growing concerns over TiO_2 and its toxicity, especially food grade titanium dioxide (E171) (Han et al., 2021; Rodríguez-Ibarra et al., 2022; Fiordaliso et al., 2022). Recently, TiO_2 was barred from food products and animal feed in Europe (May 2021 and June 2021 – European Food Safety Authority (EFSA)). Recent research has focused on iron titanate (Fe_2TiO_5) nanoparticles as a biocompatible, antioxidant component of alginate films and a possible alternative to TiO_2 (Rizzotto et al., 2022). Compared to ZnO that showed cell damage at 0.5 mg/ml, even at 2 mg/ml Fe_2TiO_5 caused no damage to human Caco-2 epithelial cells.

Metal oxide nanoparticles can be produced by a variety of synthesis methods that influence the resulting NP structure, morphology and other properties (Nikolic et al., 2021; Bandeira et al., 2020). Green synthesis involves exploiting non-toxic and eco-friendly precursors in the process to reduce the need for toxic chemicals and high temperature, energy or pressure. This results in a more environmentally friendly method, lower production cost and less dangerous or hazardous waste (Verma, Pathak, Srivastava, Prawer, & Tomljenovic-Hanic, 2021; Jeevandanam et al., 2022). Different plant and microbial (yeast, algae, bacteria, fungi) extracts have been applied as precursors in the green synthesis process (Jeevandanam et al., 2022; Singh et al., 2018). Plant extracts contain phytochemicals that are safe, cheap and readily available reducing and capping agents for bottom-up green synthesis of metal oxide NPs. Water is most often used as the solvent. This type of synthesis process can be easily scaled up to industrial level. NPs obtained using green synthesis procedures have demonstrated increased biocompatibility and improved properties for a wide field of applications, including energy storage, waste water treatment, environmental protection and remediation and other bio-related applications (Yuliarto et al., 2019; Verma et al., 2021; Salama & Abdel Aziz, 2023). Thus, for example ZnO NPs with varied morphology and properties have been produced using green synthesis involving different biological extracts, zinc precursors and modifications of the procedure including variations in reaction pH, time and temperature (Bandeira et al., 2020; Mallakpour, Sirous & Hussain, 2021). Uniform and non-agglomerated ZnO NPs were obtained using *Coriandrum sativum* extract by a simple process not requiring a calcination step (Salama & Abdel Aziz, 2023). Biodegradable waste such as fruit and vegetable peel is an affordable and renewable source of extracts used in green synthesis of metal oxides (Aswathi et al., 2022; Sani et al., 2023). Utilization of such waste products reduces environmental pollution. One such source is citrus peel from oranges and lemons that accounts for up to 50–60% of the total fruit weight (Aswathi et al., 2022). Application of dried and ground lemon peel powder in the synthesis process resulted in ZnO NPs with improved surface and optical properties (Abarna et al., 2019), while synthesis of ZnO NPs using orange fruit peel extract gave enhanced antibacterial activity (Thi et al., 2020).

In this work, a novel active packaging film was developed by incorporation into alginate of ZnO and Fe_2TiO_5 nanoparticles produced by green synthesis using citrus peel extract. A preservation study of fresh strawberry fruit was performed. Previous research showed that Fe_2TiO_5 nanoparticles provide strong antioxidant activity and high safety with no measurable migration of metal ions from the alginate films to food simulants (Rizzotto et al., 2022). The aim of this study was to improve the functionality of this packaging using ZnO nanoparticles that show high antibacterial activity. The influence of both metal oxide nanoparticle components on fruit spoilage was examined. The study includes detailed structural and morphological characterization of the synthesized nanoparticles and analysis of antimicrobial properties against gram positive and gram negative pathogens: *Salmonella enteritidis*, *Staphylococcus aureus*, *Escherichia coli* and *Enterococcus faecalis*. Synergy of the favourable antimicrobial properties of ZnO with the high antioxidant activity of Fe_2TiO_5 was aimed to achieve a prospective safe and active packaging solution.

2. Material and methods

2.1. Materials, reagents and solutions

The following precursors (all produced by Sigma Aldrich (Darmstadt, Germany)) were used for synthesis of ZnO, Fe_2TiO_5 NPs and film preparation: iron(III) nonahydrate ($Fe(NO_3)\cdot 9\ H_2O$, ACS reagent, purity $\geq$ 98%), zinc nitrate hexahydrate ($Zn(NO_3)_2\cdot 6\ H_2O$, reagent grade, purity $\geq$ 98%), titanium isopropoxide ($Ti(OCH)(CH_3)_2$, purity 98%), oxalic acid (Puriss, purity $\geq$99%), sodium alginate, glycerol and calcium chloride dehydrate (puriss p.a. ACS reagent). Tryptic soy agar (TSA), tryptic soy broth (TSB) and 2,3,5-triphenyl tetrazolium chloride (TTC) were procured from Sigma Chemical Co. (St. Louis, MO, USA).

2.2. Green synthesis of ZnO nanoparticles

Mandarin orange (*Citrus reticulata*) peel was collected from mandarin oranges purchased at a local market. They were dried for 3–5 days under direct natural sunlight, and blended into fine powder. 1 g of powder was placed in a glass container with 50 ml of deionized water, kept stirring for 3 h and then transferred to a water bath where mixing continued at 60 °C for 1 h. Finally, the solution was passed through filter paper and the obtained aqueous mandarin orange extract was stored in a refrigerator. ZnO nanoparticles were produced using the green synthesis method described by Nava et al. (2017). Thus, 2 g of $Zn(NO_3)_2\cdot 6\ H_2O$ was mixed with 42.5 ml of mandarin extract and stirred for 1 h at 60 °C on a magnetic hotplate until evaporation and powder formation were complete. A detailed scheme of the particle preparation is shown in Fig. S1.

2.3. Green synthesis of Fe_2TiO_5 nanoparticles

Lemon (*Citrus limon*) peel was collected from spent lemons purchased at a local market. Pectin was extracted by boiling finely chopped up peel in water (1 kg peel, 3 l water) for 30 min. The solution was passed through filter paper and the pale-yellow aqueous lemon peel extract was stored in a refrigerator. This extract was used in green synthesis of Fe_2TiO_5. It replaced other chemicals commonly used in Fe_2TiO_5 synthesis as surfactants or capping agents (Ramezani, Davoodi, Malekizad, & Hosseinpour-Mashkani, 2015; Vasiljevic et al., 2020) and thus this method can be classified as green synthesis (Talebi et al., 2016). The precursors, 4 g $Fe(NO_3)\cdot 9\ H_2O$ and 1.4 g $Ti(OCH)(CH_3)_2$ were separately dissolved in 20 ml of ethanol. Lemon peel extract (30 ml) was added and the mixture stirred for 30 min on a magnetic hotplate. Afterwards, oxalic acid solution in ethanol was added by continuous stirring until a thick gel formed. The solution pH was around 2. The obtained gel was further heated to 150 °C in an oven where the gel dried and converted into powder form. The obtained powder was ground and then calcined at 750 °C for 3 h in a chamber furnace to obtain Fe_2TiO_5 nanoparticles. A detailed scheme of the particle preparation is shown in Fig. S2.

2.4. Characterization of ZnO and Fe_2TiO_5 nanoparticles

Study of the structure and morphology of ZnO and Fe_2TiO_5 NPs included recording X-ray diffraction (XRD) patterns on a Rigaku Ultima IV diffractometer (Tokyo, Japan) range 10–90°, step 0.05 s, acquisition rate 1°/min, gathering Fourier Transform Infrared (FTIR) spectra in the range 400–4000 cm^{-1} with a resolution of 4 cm^{-1} on a Perkin Elmer Spectrum Two (Waltham, MA, USA), observing field emission electron microscopy (FESEM) images on a FEI Quanta FEG (Thermo Fischer Scientific, Waltham MA, USA), and transmission electron microscopy (TEM) images on a FEI TECNAI F20 (Thermo Fischer Scientific, Waltham MA, USA) with an X-FEG emitter operated at 200 kV and taken with a Gatan Rio 16 CMOD camera, obtaining STEM images using a Gatan DigiSTEM II and a high angle annular dark field (HAADF) detector and collecting diffuse reflectance spectra (DRS) on a Shimadzu UV-2600 through an ISR Plus ISA (Kyoto, Japan), range 200–1400 nm. Absorbance spectra of the NPs were calculated as the Kubelka-Munk transformation of the measured DRS.

2.5. Synthesis and characterization of ZnO, Fe_2TiO_5 alginate films

Alginate film was prepared using the method previously described in (Vizzini et al., 2020; Rizzotto et al., 2022). Then ZnO, Fe_2TiO_5 and ZnO/Fe_2TiO_5 NPs were ultrasonically blended into the prepared gel. The obtained solutions were solution cast (4 ml) into Petri dishes (5 cm in diameter) and dried for 12 h at 50 °C. Film wetting (10 min) was done using 5% calcium chloride solution, followed by washing with distilled water, and subsequent drying at room temperature between two layers of thick filter paper (Whatman, Maidstone, UK). Some wrinkling was observed round the edges (as shown in Fig. S3) but it was not significant and measurements were possible.

Attenuated total reflection (ATR) Fourier transform infrared (FTIR) spectroscopy (range 400 - 4000 cm^{-1}, resolution 8 cm^{-1}) was applied to study film structure and composition with a Perkin Elmer Spectrum Two (Waltham, MA, USA), by directly measuring the films in at least three random places (Costa et al., 2018; Lopusiewicz et al., 2022). UV-Vis transmittance spectra, range 200–850 nm, step 1 nm, were recorded by placing the investigated films in a standard film sample holder using a Shimadzu UV-2600 spectrophotometer combined with an Integrating Sphere Attachment ISR-2600 Plus (Kyoto, Japan). The opacity value was calculated (Zhao, Wang & Liu, 2022): Opacity $= A_{600}/x$, with A_{600} denoting the absorbance at 600 nm and x denoting the film thickness in mm. Film transparency was determined as %*Transmittance* at 600 nm (Motelica et al., 2021). Film thickness was measured at several random positions on the films using a laboratory micrometer device and the average values were calculated (Lopusiewicz, Macieja, Sliwinski, Bartkowiak, & Roy, 2022).

The dry matter content, water solubility and swelling degree of the prepared films (specimen size 1 × 1 cm, measured in triplicate) were calculated as follows: dry matter content (%) $= m_2/m_1 \times 100$; solubility (%) $= (m_2\text{-}m_4)/m_2 \times 100$; swelling degree (%) $= (m_3\text{-}m_2)/m_2 \times 100$ using the gravimetrical procedure described by Salevic et al. (2022) where m_1 is the initial film mass, m_2 is the dry film mass, m_3 is the film mass after immersion in distilled water for 24 h and m_4 is the final dry mass, m_4.

Colour analysis of the films was performed by direct measurement with a Chroma Meter CR-400 (Konica Minolta, Japan) and a white calibration plate ($Y = 84.8$, $x = 0.3199$ and $y = 0.3377$). Each sample was measured at five random positions on the film surface. The CIELAB scale (L^*, a^*, b^*) was used to determine the colour parameters (Choi, Lee, lyu, Lee, & Han, 2022). The hue angle ($h°$) was determined as arctan (b^*/a^*), while chroma (C^*) was calculated as $(a^*2+b^*2)^{1/2}$ (Belović et al., 2014). The total colour difference (ΔE^*) was calculated as:

$$\Delta E^* = \sqrt{(L_2^* - L_1^*)^2 + (a_2^* - a_1^*)^2 + (b - b_1^*)^2} \quad (1)$$

while the whiteness index (WI) was determined as:

$$WI = 100 - \sqrt{(100 - L^*)^2 + a^{*2} + b^{*2}} \quad (2)$$

TG/DTA analysis of film samples on a 6000 TG/DTA Perkin Elmer device (Waltham, MA, USA) was utilized to study thermal degradation behaviour (heating rate 10°/min in argon gas up to 500 °C).

2.6. Antimicrobial activity

Antibacterial activity of NPs was tested in triplicate on *Salmonella enteritidis* ATCC 22076, methicillin-resistant *Staphylococcus aureus* (MRSA) ATCC 25923, *Escherichia coli* ATCC 25922, and *Enterococcus faecalis* ATCC 29212. Bacterial strains were sustained on TSA plates and retrieved by culturing in TSB. Minimum inhibitory (MIC) and minimum bactericidal (MBC) concentrations were established using the microdilution method as described previously (Klaus et al., 2015). In short: serial dilutions of NPs in TSB (0.156 mg/ml - 20 mg/ml) were prepared in flat-bottomed sterile 96-well microtiter plates (Sarstedt, Germany) and inoculated with TSB cultivated bacterial strains, incubated, followed by MIC and MBC determination with gentamicin as the positive control, bacterial dilutions in TSB as the negative control, and TSB alone as the sterility control.

2.7. Preservation study on fresh strawberry fruit

Strawberries were chosen as the target food for performing the preservation study. They are a fruit that perishes easily but is a popular and convenient healthy snack sold “ready to eat” both whole and cut (Paulsen, Barrios, & Lema, 2021; Avalos-Llano et al., 2018). Fresh strawberries were purchased from a local market store. They were washed with distilled water, dried in air at room temperature (25 °C) and then cut in half and covered with pieces of film (alginate, Fe_2TiO_5-alginate, ZnO-alginate and ZnO/Fe_2TiO_5-alginate). The study was conducted in open atmosphere at a temperature of around 18 °C and relative humidity of around 40%. Photographs were taken with a high resolution camera for 4 consecutive days to register evidence of physical deterioration, microbial and fungal infestation and growth. All experiments were done in triplicate.

2.8. Statistical analysis

Statistica software (version 6) was employed for statistical analysis of the obtained results. Analysis of variance (ANOVA), the post hoc Fisher test and Tukey honest significance difference (HSD) test at the significance threshold of $p < 0.05$ were applied to determine differences between means.

3. Results and discussion

3.1. Structure and morphology of ZnO nanoparticles

The green synthesized ZnO NPs were pale grey in colour (Fig. S1). ZnO powder is commonly white when the production route involves a calcination (annealing) stage at a high enough temperature applied for a long enough time (Thi et al., 2020). When the calcination temperature is lower and the time is shorter or this step is not applied, ZnO powder can have a different colour: black, grey, or even orange. The orange colour is caused by residues of the green synthesis process using orange peel extract (Thi et al., 2020). Our ZnO NPs were formed with no calcination step, hence their pale grey colour. The XRD pattern (Fig. 1a) revealed wide pure wurtzite $P6_3mc$ phase ZnO crystalline lattice peaks (JCPDS card 36–1451). Wide peaks are indicative of nanoparticles and the TEM images (Figs. 1b and 1f) corroborate this (average NPs 10 nm). Selected area diffraction (SAED) analysis of a number of HRTEM images of the synthesized ZnO NPs validated XRD pattern analysis. An example is the

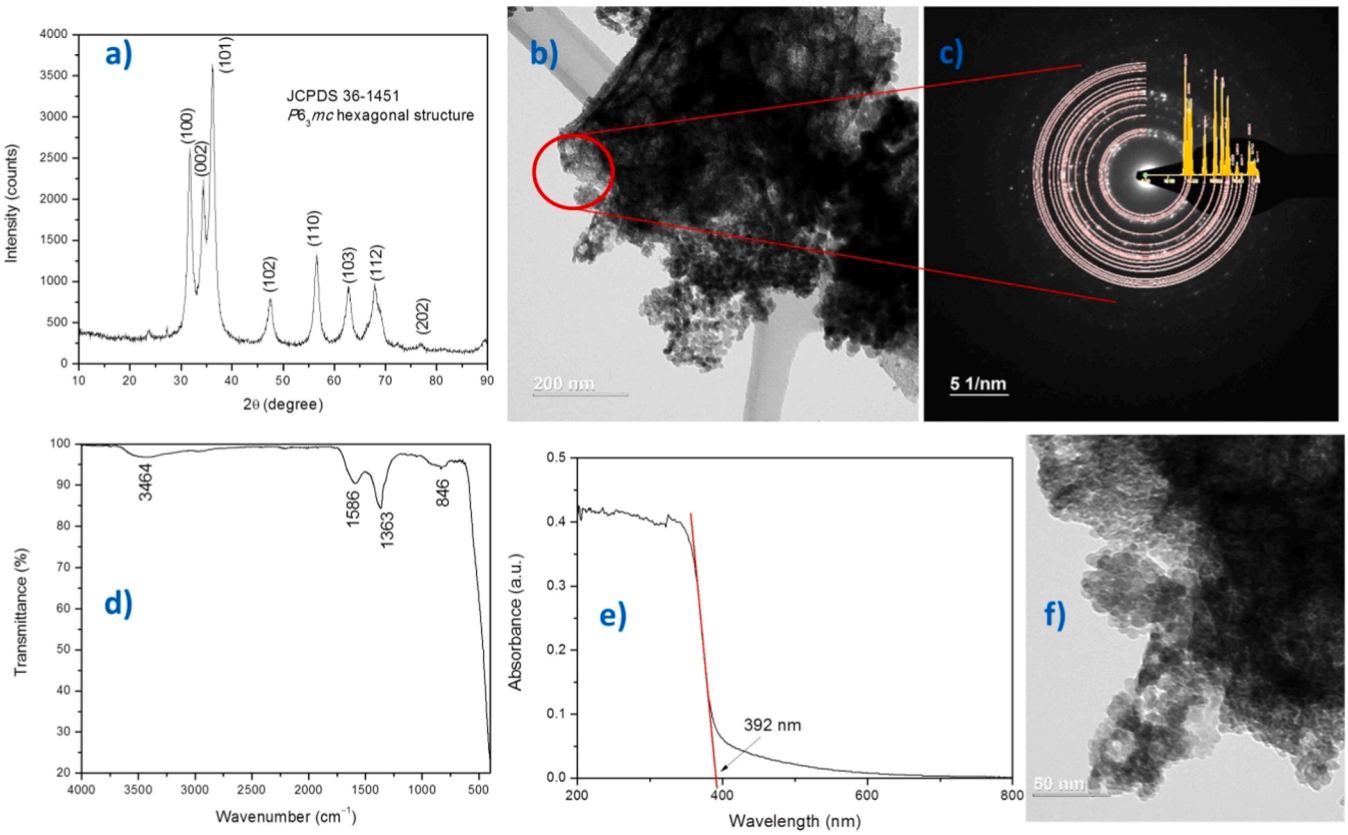

Fig. 1. XRD pattern (a), TEM image with phase analysis area marked as a red circle (b), SAED pattern of the red marked circle area and corresponding ZnO phase rings (c), FTIR (d), and UV-Vis absorbance with the red line and arrow showing the approximated excitation wavelength of 392 nm (e) spectra and higher magnification TEM image (f) of ZnO NPs.

area selected in the red circle in Fig. 1b and the corresponding SAED in Fig. 1c revealing diffraction ring patterns characteristic for NPs allocated to ZnO (JCPDS 36–1451). The structure of ZnO NPs was further evaluated by FTIR (Fig. 1d) revealing low intensity peaks (≈ 3464 cm^{-1}) typical for H_2O vibrations on the NP surface (Thi et al., 2020). The other notable vibrations in the spectrum are due to traces of mandarin orange extract used in the green synthesis, namely aromatic C═C bending at ≈ 1586 cm^{-1} (Omran, Aboelazayem, Nassar El-Salamony, & El-Gendy, 2021), aromatic ring C-C stretching at ≈ 1363 cm^{-1} (Luque at al., 2018) and functional vibrations of Zn-OH and C-H aromatic bands at ≈ 846 cm^{-1} (Thi et al., 2020; Luque et al., 2018). A broad band (200–400 nm, UV region) and approximated excitation wavelength of 392 nm was revealed in the determined ZnO absorbance spectrum (Fig. 1e) in correlation with previous findings (Motelica et al., 2021).

3.2. Structure and morphology of Fe_2TiO_5 nanoparticles

The green synthesized Fe_2TiO_5 NPs were light warm brown in colour due to the iron content in the powder (Fig. S2). Well-defined pure Fe_2TiO_5 phase crystalline peaks (orthorhombic *Cmcm* JCPDS card 76–1158) are revealed in the measured structure (XRD pattern) in Fig. 2a. Morphological investigation of Fe_2TiO_5 NPs (FESEM Fig. 2b, HRTEM Fig. 2c) revealed clusters of Fe_2TiO_5 NPs confirming previous morphological examinations of this material (Vasiljevic et al., 2020). Due to the calcination step in the synthesis procedure the average particle size for Fe_2TiO_5 (50 nm) was larger than for ZnO in line with previous research (Rizzotto et al., 2022). The study of HRTEM images further verified the presence of only Fe_2TiO_5 NPs in the synthesized powder. An example is given in Fig. 2c, where analysis of the marked part of the image using FFT (Fast Fourier Transform) provided the indicated lattice spacing of 0.35 nm that can be matched to the highest intensity (110) peak (shown in the XRD in Fig. 2a). Further structural analysis by FTIR (Fig. 2d) revealed only vibrations (≈ 800, 661, 618 and 433 cm^{-1}) deriving from Fe and Ti−O group vibrations of Fe_2TiO_5, in correlation with previous findings (Rizzotto et al., 2022). A marked wide light absorption spanning UV and visible portions of the spectrum up to 600 nm, with an excitation band at 571 nm, were noted for the absorbance spectrum (Fig. 2e) of the produced Fe_2TiO_5 NPs and can be correlated with similar spectra of Fe_2TiO_5 NPs and nanofibers (Vasiljevic et al., 2020; Vasiljevic et al., 2021). The absorption intensity was in line with values determined for Fe_2TiO_5 nanofibers fabricated at higher temperatures, such as 700 and 750 °C.

3.3. Antimicrobial activity of ZnO and Fe_2TiO_5 nanoparticles

ZnO NPs inhibited bacterial growth of all assessed strains but effectiveness was strain dependent (Table 1). Thus, antibacterial activity was similar against both Gram-negative species tested (*E. coli* and *S. enteritidis),* but quite different for the two Gram-positive bacteria. Indeed, the lowest ZnO NP MIC and MBC values were found against the MRSA strain, relatively resilient to gentamicin, while ZnO NPs had the least influence on the development of *E. faecalis*. In the case of Fe_2TiO_5 NPs, the MIC activity was above the tested maximal 20 mg/ml and MBC was not established for both Gram-positive and Gram-negative species, confirming previous findings that Fe_2TiO_5 shows no toxicity towards bacterial cells (Rizzotto et al., 2022).

Even though the ZnO NP mode of action on microorganisms has not been completely elucidated, ZnO NPs with diverse morphologies have been shown to kill many different microorganisms (Slavin, Asnis, Häfeli, & Bach, 2017; Azam et al., 2012; Gudkov et al., 2021; da Silva et al., 2019; Zanet et al., 2019). One crucial parameter seems to be NPs size, while the second is the type of targeted bacterial cell. The larger surface

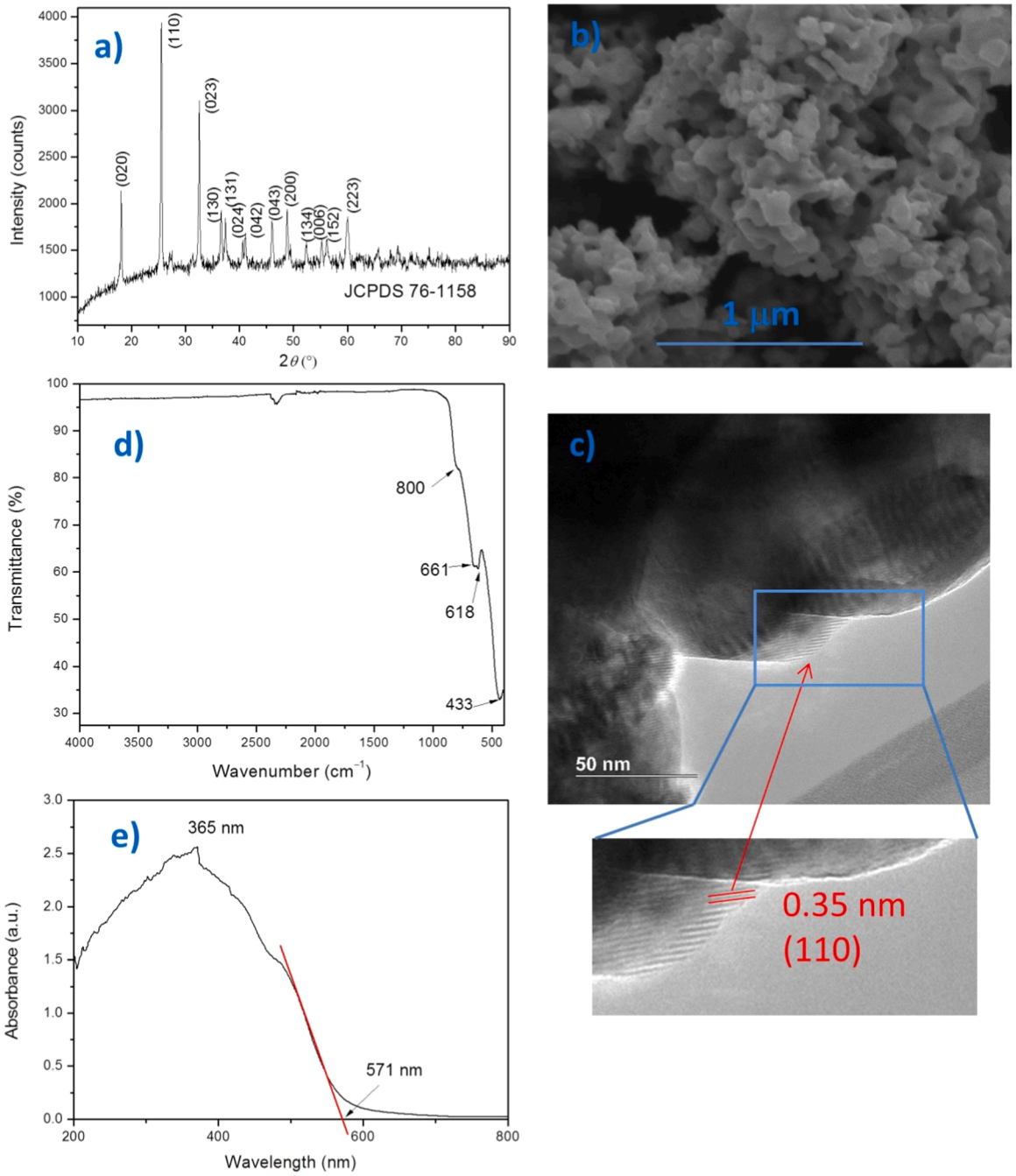

Fig. 2. XRD pattern (a), FESEM image (b), HRTEM image with the blue rectangle marking the magnified part shown below that was analysed by Fast Fourier Transform with the red arrow depicting the lattice spacing of 0.35 nm that can be matched to the highest intensity X-ray diffraction peak (110) of Fe_2TiO_5 orthorhombic *Cmcm* crystalline lattice (c), FTIR transmittance spectrum with main peaks marked with arrows (d) and UV-Vis absorbance spectrum absorbance with the red line and arrow showing the approximated excitation wavelength of 571 nm (e) of Fe_2TiO_5 NPs.

volume and multiple ions to interact with the medium or bacterial cells point to higher reactivity of smaller NPs. The estimated average size of ≈ 10 nm of the ZnO NPs synthesized in this work ensured a large surface volume and also internalization into bacterial cells combined with interactions with intracellular molecules (Stankic et al., 2016; Staroń & Długosz, 2021). High antibacterial effectiveness of ZnO NPs against both Gram-positive and Gram-negative bacterial strains tested suggests that they may exert multiple modes of action. In keeping with this, *E. faecalis* was affected the least and MBC was not established for the tested range of ZnO concentrations. The sensitivity of Gram-negative species to ZnO NPs may be due to the lipopolysaccharide and peptidoglycan thin layer design allowing easy introduction of toxic Zn^{2+}-ions and reactive oxygen species (ROS) originating from ZnO NPs (Slavin et al., 2017; Zanet et al., 2019). Moreover, da Silva et al. (2019) showed that it may be due to the NP morphology. However, a Gram-positive species, *Bacillus subtilis* reacted notably to Mg-doped ZnO NPs (Auger et al., 2019) which triggered multiple mechanisms of bacteriostatic and bactericidal activity and involved perturbation in bacterial stress responses, biofilm formation, motility and chemotaxis, purine metabolism and translation.

3.4. Structure and properties of alginate-ZnO/Fe_2TiO_5 films

As presented in Fig. 3 all produced films were transparent. The films containing ZnO and/or Fe_2TiO_5 NPs were yellow-grey to light brown.

Table 1
Antimicrobial activity of ZnO nanoparticles expressed as MIC and MBC determined by the broth microdilution method.

	ZnO		gentamicin	
	MIC (mg/ml)	MBC (mg/ml)	MIC (mg/ml)	MBC (mg/ml)
***S. enteritidis* ATCC 22076**	1.25	20	0.024	0.024
***S. aureus*, MRSA, ATCC 25923**	0.156	1.25	2.5	2.5
***E. coli*, ATCC 25922**	1.25	10	0.0097	0.0097
***E. faecalis*, ATCC 29212**	10	-	0.078	0.156

- not achieved. There are no standard deviations since there was no difference between repetitions.

The measured and calculated colour parameters are given in Table 2. Compared to the colour values measured for the white plate ($L^* = 93.23$, $a^* = -0.196$ and $b^* = 4.728$), the pure alginate film cross-linked with $CaCl_2$ showed a slight change, namely a decrease in the lightness value (L^*), an increase in the redness/greenness parameter (a^*) and decrease in the yellowness/blueness parameter (b^*). The colour parameters of the Fe_2TiO_5-alginate films differed the most from the pure alginate film with the lowest L^* and highest a^* and b^* indicating noticeable colouring of the film with the highest total colour difference (ΔE^*) and lowest whiteness value (WI). The ZnO-alginate films were the most similar to pure alginate films, with a slightly lower L^* and higher a^* and b^*. This difference was statistically significant as shown in Table 2, reflecting the yellow-grey colour shown in Fig. 3a. The ZnO/Fe_2TiO_5-alginate film had colour parameter values in between the ZnO-alginate and Fe_2TiO_5-alginate films, indicating the combined influence of the two different added nanoparticles. These films also showed the highest standard deviations indicating that the Zn^{2+}, Fe^{3+} and Ti^{4+} ions were distributed somewhat non-uniformly across the alginate film. Regarding the CIE parameters h° and C^* the hue was similar for all three films containing nanoparticles when compared to pure alginate film. Nevertheless, the difference was statistically significant, as shown in Table 2. The chroma C^* values also differed significantly, with the lowest obtained for pure alginate film and the highest for Fe_2TiO_5-alginate film.

The UV-Vis transmittance spectrum measured for alginate film (Fig. 3b) had transmittance of 76.48% at 300 nm, increasing to 86.61% at 400 nm, 88.44% at 500 nm and reaching 89.4% at 800 nm., in line with previous alginate film research (Bai et al., 2020). For films containing NPs, the transmittance was generally lower. Composite NP-alginate films have previously shown lower transmittance which was connected with the NP content in the films and film thickness (Lopusiewicz et al., 2022; Motelica et al., 2021). UV light protection and light barriers are needed for quality food preservation in order to obstruct nutrient and vitamin decomposition and oxidation induced by light. ZnO has been employed before for this end (Motelica et al., 2021; Lopusiewicz et al., 2022). For Fe_2TiO_5 –alginate films transmittance was overall lower, changing from 38.54% at 300 nm, 41.81% at 400 nm, and 50.28% at 500 nm to 71.74% at 800 nm. These films offered some UV protection. The ZnO alginate films showed good UV protection, taking into account the optical properties of ZnO NPs displayed in Fig. 1e. The transmittance was 6.9% at 300 nm, increasing to 32.80% at 400 nm and 62.99% at 800 nm. In the case of ZnO/Fe_2TiO_5 – alginate films, the change in transmittance echoed the presence of both types of NPs, with transmittance of 25.19% at 300 nm offering UV light barrier protection,

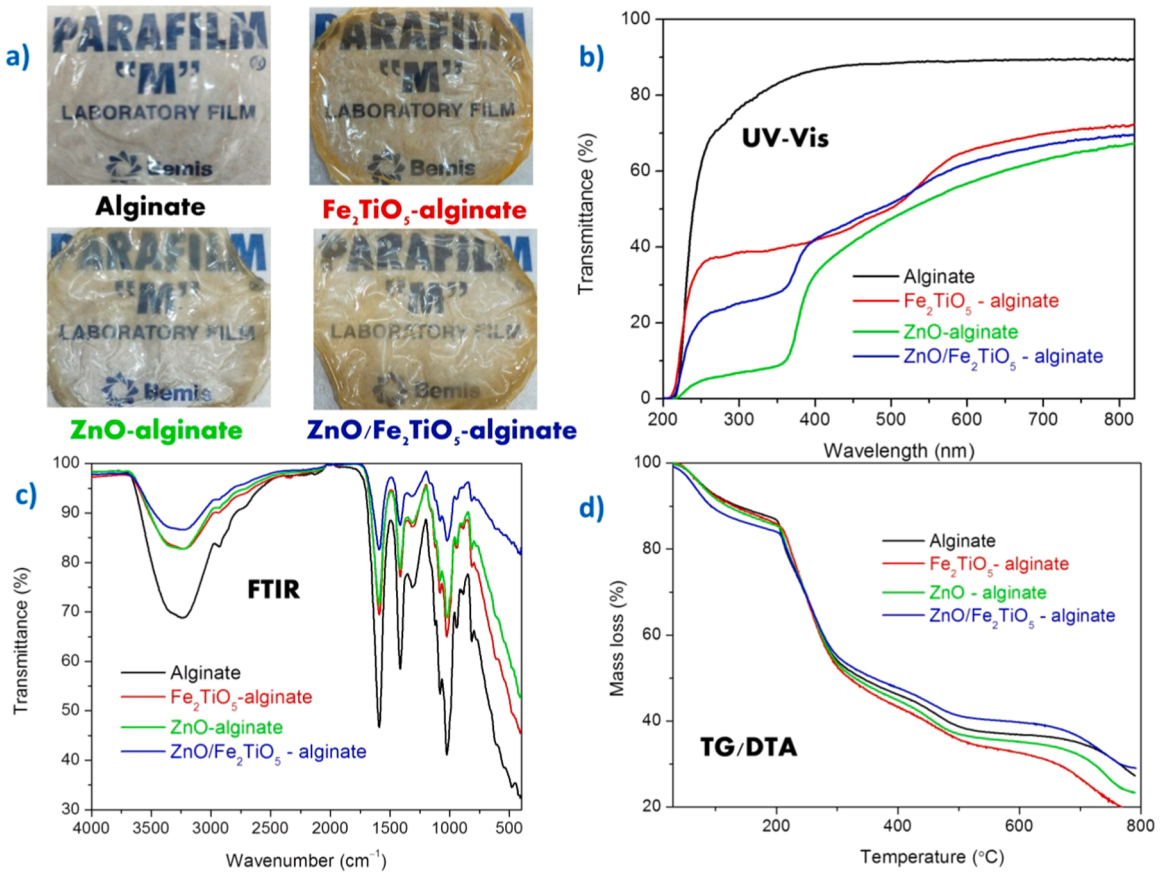

Fig. 3. Transparency (a), UV-Vis transmittance spectra (b), TG/DTA curves (c) and FTIR spectra (d) of alginate, Fe_2TiO_5 – alginate, ZnO-alginate and ZnO/Fe_2TiO_5 – alginate films.

Table 2
Colour parameters (L^*, a^*, b^*, h°, C^*, WI and ΔE^*), transparency, opacity, dry matter content, solubility and swelling degree of alginate, Fe_2TiO_5-alginate, ZnO-alginate and ZnO/Fe_2TiO_5 – alginate films.

Parameters	Sample			
	Alginate	Fe_2TiO_5-alginate	ZnO-alginate	ZnO/Fe_2TiO_5 - alginate
***x* (mm)**	0.32 ± 0.04	0.31 ± 0.02	0.33 ± 0.02	0.33 ± 0.02
L*	89.50 ± 0.63^a	79.16 ± 0.45^d	87.07 ± 1.69^b	80.95 ± 4.44^c
a*	-0.43 ± 0.03^d	8.49 ± 0.27^a	0.63 ± 0.05^c	4.51 ± 0.84^b
b*	8.26 ± 0.43^d	32.62 ± 0.83^a	11.81 ± 0.27^c	25.79 ± 2.71^b
h°	-1.518 ± 0.004^d	1.316 ± 0003^c	1.517 ± 0.003^a	1.399 ± 0.015^b
C*	8.27 ± 0.42^d	33.70 ± 0.87^a	11.83 ± 0.27^c	26.18 ± 2.81^b
WI	86.63 ± 0.66^a	60.37 ± 0.96^d	82.47 ± 0.31^b	67.61 ± 3.26^c
ΔE*	5.15 ± 0.65^d	32.42 ± 0.97^a	9.42 ± 0.31^c	24.83 ± 3.29^b
Transparency (%)	89.01	65.26	56.76	62.01
Opacity (%)	0.16	0.59	0.74	0.63
Dry matter content (%)	83.13 ± 0.86^a	83.47 ± 0.81^a	82.72 ± 1.15^a	83.65 ± 0.51^a
Solubility (%)	4.26 ± 0.44^{a,b}	2.77 ± 0.31^b	7.49 ± 1.60^a	7.12 ± 2.09^a
Swelling degree (%)	263.08 ± 30.68^a	241.36 ± 72.91^a	308.08 ± 77.41^a	177.90 ± 32.14^a

Values are given as means ± standard deviation. Means with different letters (a, b, c and d) are significantly different at $p < 0.05$ (compared to other variants within the groups)

increasing to 42.08% at 400 nm and 69.32% at 800 nm, showing similar transparency in the visible domain to ZnO films. The measured transparency and calculated opacity values (at 600 nm) are shown in Table 2. Opacity varied between 0.16 for pure alginate film and 0.74 for ZnO-alginate films (Table 2). In all cases the films were fairly transparent, and the opacity was similar to other alginate films incorporating ZnO NPs (Motelica et al., 2021; Aziz & Salama, 2022).

Wetting the films with $CaCl_2$ ensured egg-box model type infiltration of calcium (Ca^{2+}) ions into the films (Cao, Lu, Mata, Nishinari, & Fang, 2020; Wang, Wan, Wang, Li, & Zhu 2018). Alginate polymer chains in composite films are organized around the NPs. Addition of Ca^{2+} ions promoted further film strengthening (Motelica et al., 2021). The dry matter content in all film samples was comparable and relatively high, displaying dominant dependence on the $CaCl_2$ cross-linked alginate films rather than on the presence of ZnO and/or Fe_2TiO_5 NPs. As shown in Table 2 it varied between 82.72% and 83.65% creating moisture contents between 16.35% and 17.28%. Similar values were obtained before for alginate films (Alboofetileh et al., 2013).

The swelling degree varied depending on film composition (Table 2). All films swelled but conserved their integrity after 24 h agitated immersion in water. Pure and ZnO-alginate films displayed swelling values similar to those noted earlier (Wang et al., 2019). A similar swelling percentage was obtained by Motelica et al. (2021). Incorporation of Fe_2TiO_5 in the alginate matrix slightly reduced the degree of swelling, while the combination of ZnO and Fe_2TiO_5 NPs led to even lower values. Swelling degree has been linked with the extent of crosslinking (Choi et al., 2022; Costa et al., 2018). Thus, Costa et al. (2018) determined that adding a certain concentration of $CaCl_2$ increases the number of guluronic (G) blocks of alginate linked with calcium ions resulting in a high swelling degree. They explained this phenomenon with an "egg-box" model that enables film resistance to be high enough not to dissolve in water, but with strands still available for water uptake. Further increase of $CaCl_2$ concentrations led to more bonds and fewer strands available for swelling and thus a decrease in the swelling degree. Quadrado and Fajardo (2017) showed that cross-linking alginate with Fe^{3+} ions resulted in a decrease in swelling degree. This was attributed to stronger reactions of Fe^{3+} ions with carboxyl and hydroxyl functional groups of alginate that lessened interaction of hydrophobic sites with water molecules leading to restricted network expansion. This phenomenon can explain the lower swelling degree noted for Fe_2TiO_5-alginate films, as they contain Fe^{3+} and Ti^{4+} ions as well as Ca^{2+} in the alginate matrix. Wang et al. (2019) showed that incorporation of ZnO and the presence of Zn^{2+} ions in the alginate matrix, besides Ca^{2+}, resulted in an increased swelling degree, and this can explain the results obtained for ZnO-alginate films. In the case of the ZnO/Fe_2TiO_5 – alginate films, where the lowest swelling degree was obtained, the combined influence of metal ions originating from the two types of nanoparticles, i.e. Fe^{3+}, Ti^{4+} and Zn^{2+} combined with Ca^{2+}, led to an even larger level of reaction of metal ions with carboxyl and hydroxyl groups resulting in marked restriction in network expansion and a low swelling degree.

Film solubility in distilled water was low, and below 8% for all film samples. According to Roger, Talbot, and Bee (2006) low solubility of alginate films may be accomplished with a high concentration of Ca^{2+} ions. Elevated crosslinking levels obstruct alginate dissolution, and lessen swelling and film solubility (Choi et al., 2022; Costa et al., 2018). The presence of different types of NPs led to some variation in film solubility, with the lowest value of 2.77% obtained for Fe_2TiO_5-alginate films, and the highest of 7.49% for ZnO-alginate films.

Peaks characteristic for alginate films can be identified in the FTIR spectra, as shown in Fig. 3c (Dojcinovic, Vasiljevic, Kovac, Tadic, & Nikolic, 2021; Giz et al., 2020). The creation of new bonds or disappearance of bonds usually present in alginate film was not recorded after the addition of ZnO or Fe_2TiO_5 NPs. Only small differences in the range 800–400 cm^{-1} mirrored the presence of Zn−O and/or Fe−O and Ti−O metal ion bands in the alginate film (Motelica et al., 2021; Rizzotto et al., 2022), although variation in peak intensity and minor shifts of some peaks characteristic for alginate films were noted. The intense pronounced band at ≈ 3255 cm^{-1} is due to vibration of −OH groups. The shoulder at ≈ 2926 cm^{-1} (alginate film) from −CH stretching vibrations (Lopusiewicz et al., 2022) revealed a minor shift due to the presence of ZnO and/or Fe_2TiO_5 NPs to around 2933 cm^{-1}. The characteristic vibrations for −CO in COO^- groups (asymmetric and symmetric) were noted at ≈ 1590 cm^{-1} and 1413 cm^{-1}, respectively. The pronounced band at around 1024 cm^{-1} (minor shift to 1022 cm^{-1} for ZnO-alginate and ZnO/Fe_2TiO_5-alginate films) and shoulder at around 1078 cm^{-1} (minor shift to 1080 cm^{-1} for ZnO-alginate and ZnO/Fe_2TiO_5-alginate films) are ascribed to C−O−C bond stretching vibrations (Giz et al., 2020), while the range 800–1000 cm^{-1} is the region of polysaccharide structures (Rizzotto et al., 2022).

Thermal stability of neat alginate, Fe_2TiO_5-alginate, ZnO-alginate and ZnO/Fe_2TiO_5- alginate composite films, followed using TG/DTA analysis, manifested two stage thermal decomposition (Fig. 3d). The first stage of weight loss of 15% occurred at around 100 °C and was due to elimination of adsorbed water. The second thermal degradation step took place at 200–360 °C and is caused by alginate thermal decomposition and glycerol evaporation (Shankar, Kasapis, & Rhim, 2018). Thermal stability of alginate films was to a certain degree enhanced by incorporation of ZnO and Fe_2TiO_5 NPs, as shown by the small difference in the TGA curves obtained. After the final thermal decomposition at 800 °C, the final residue for neat alginate film was 27.3%. This increased to 29.28% when the mixture of ZnO and Fe_2TiO_5 NPs was incorporated, confirming previous findings for composite alginate-NP films (Dash, Ali, Das, & Mohanta, 2019).

3.5. Preservation of fresh strawberry fruit

This study was done on freshly cut strawberries in open air conditions in order to verify the preservative effect of alginate, Fe_2TiO_5-alginate, ZnO-alginate and ZnO/Fe_2TiO_5 – alginate films on a food sample sensitive to oxidation (Fig. 4). Freshly cut strawberries

deteriorate visibly in open air. On the control sample this started on day 1 with some edge curling, while such edge spoilage was less noticeable when films were applied. More perceptible deterioration commenced on day 2, when the control sample revealed observable fruit tissue deterioration. The alginate film covered sample also displayed evident edge spoilage and some fruit tissue change on day 2. This was also observed for ZnO-alginate samples, while Fe_2TiO_5 – alginate and ZnO/Fe_2TiO_5 – alginate samples displayed only slight edge discoloration. On day 3 there was evident spoilage and fungal growth on the control sample, while those covered by films were less affected. The alginate and ZnO-alginate protected samples showed more observable spoilage than the Fe_2TiO_5–alginate and ZnO/Fe_2TiO_5–alginate film protected samples on day 3. On day 4 tissue was discoloured more in the strawberry sample covered with ZnO-alginate film when compared to the Fe_2TiO_5 – alginate sample. Overall strawberry protection was most improved by the ZnO/Fe_2TiO_5 – alginate film, indicating the beneficial influence of both types of NPs incorporated into the alginate matrix.

4. Conclusions

Active alginate films incorporating antioxidant Fe_2TiO_5 and antimicrobial ZnO nanoparticles were obtained using the solution casting method. Pure phase ZnO and Fe_2TiO_5 nanoparticles (with particle sizes of 10 and 50 nm, respectively) were obtained by green synthesis using citrus peel extract. The presence of ZnO and Fe_2TiO_5 nanoparticles in the film resulted in a synergistic effect, giving the lowest swelling degree, improved thermal stability, UV light protection, good transparency and opacity. When the protective activity of alginate packaging films containing ZnO NPs and Fe_2TiO_5 NPs separately or as a mixture was tested on freshly cut strawberries, protection was most enhanced by the ZnO/Fe_2TiO_5 – alginate film.

The results of this study provide a comprehensive view of various aspects of reinforcement of alginate films with ZnO and Fe_2TiO_5 NPs. Both nanoparticles may also be applicable for reinforcement of other biodegradable and environmentally friendly green polymers, such as

Fig. 4. Preservation study of freshly cut strawberry halves.

chitosan or zein. However, to achieve the ultimate goal of a highly efficient and safe food packaging material, the next challenging issue will consist of assessing and establishing the fate of metal oxide NPs obtained by green synthesis after release into the intestinal tract or the environment. Such further study is necessary prior to use in actual food systems.

CRediT authorship contribution statement

Jasmina Vidic: Writing – review & editing, Writing – original draft, Conceptualization. **Maria Vesna Nikolic:** Writing – review & editing, Writing – original draft, Visualization, Supervision, Investigation, Data curation, Conceptualization. **Goran Miskovic:** Writing – review & editing, Resources, Investigation. **Nenad B. Tadic:** Writing – review & editing, Investigation. **Milena P. Dojcinovic:** Writing – review & editing, Investigation. **Zorka Z. Vasiljevic:** Writing – review & editing, Visualization, Methodology, Investigation, Formal analysis, Data curation, Conceptualization. **Jovana Vunduk:** Writing – review & editing, Investigation, Formal analysis, Data curation.

Declaration of Competing Interest

The authors declare the following financial interests/personal relationships which may be considered as potential competing interests: Jasmina Vidic reports administrative support and travel were provided by European Commission.

Data Availability

Data will be made available on request.

Acknowledgement

We would like to thank Prof. Steva Levic from the Faculty of Agriculture, University of Belgrade, for colour measurements of our films, Prof. Goran Grubic for help with statistical analysis and Dr. Judith Anne Nikolic for proofreading the paper and correcting the language. Z.Z.V, M.P.D and M.V.N acknowledge the funding grant 451-03-66/2024-03/200053 and J. Vunduk the grant 451-03-66/2024-03/200051 from the Ministry for Science, Technology Development and Innovations of the Republic of Serbia. J. Vidic acknowledges European Union support through the Horizon 2020 research and innovation programme under the Marie Sklodowska-Curie grant agreement 872662 (IPANEMA).

Appendix A. Supporting information

Supplementary data associated with this article can be found in the online version at doi:10.1016/j.fpsl.2024.101280.

References

Abarna, B., Proethi, T., & Rajaraswary, G. R. (2019). Lemon peel guided sol-gel synthesis of visible light active nano zinc oxide. *Journal of Environmental Chemical Engineering, 7*, Article 102742. https://doi.org/10.1016/j.jece.2018.10.056

Ahmad, A., Qurashi, A., & Shehan, D. (2023). Nano-packaging – Progress and future perspectives for food safety and sustainability. *Food Packaging and Shelf Life, 35*, Article 100997. https://doi.org/10.1016/j.fpsl.2022.100997

Alboofetileh, M., Rezaei, M., Hosseini, H., & Abdollahi, M. (2013). Effect of montmorillonite clay and biopolymer concentration on the physical and mechanical properties of alginate nanocomposite films. *Journal of Food Engineering, 117*, 26–63. https://doi.org/10.1016/j.jfoodeng.2013.01.042

Aswathi, V. P., Meera, S., Ann Maria, C. G., & Nidhin, M. (2022). Green synthesis of nanoparticles from biodegradable waste extracts and their applications: a critical review. *Nanotechnology for Environmental Engineering*. https://doi.org/10.1007/s41204-022-00276-8

Auger, S., Henry, C., Péchaux, C., Lejal, N., Zanet, V., Nikolic, M. V., Manzano, M., & Vidic, J. (2019). Exploring the impact of Mg-doped ZnO nanoparticles on a model soil microorganism Bacillus subtilis. *Ecotoxicology and Environmental Safety, 182*, Article 109421. https://doi.org/10.1016/j.ecoenv.2019.109421

Avalos-Llano, K. R., Martin-Belloso, O., & Soliva-Fortuny, R. (2018). Effect of pulsed light treatments on quality and antioxidant properties of fresh-cut strawberries. *Food Chemistry, 264*, 393–400. https://doi.org/10.1016/j.foodchem.2018.05.028

Azam, A., Ahmed, A. S., Oves, M., Khan, M. S., Habib, S. S., & Memic, A. (2012). Antimicrobial activity of metal oxide nanoparticles against Gram-positive and Gram-negative bacteria: a comparative study. *International Journal of Nanomedicine, 7*, 6003–6009. https://doi.org/10.2147/IJN.S35347

Aziz, M. S. A., & Salama, H. E. (2021). Developing multifunctional edible coatings based on alginate for active food packaging. *International Journal of Biological Macromolecules, 190*, 837–844. https://doi.org/10.1016/j.ijbiomac.2021.09.031

Aziz, M. S. A., & Salama, H. E. (2022). Development of alginate-based edible coatings of optimized UV-barrier properties by response surface methodology for food packaging applications. *International Journal of Biological Macromolecules, 212*, 294–302. https://doi.org/10.1016/j.ijbiomac.2022.05.107

Bai, Y., Zhao, Y., Li, Y., Xu, J., Fu, X., Gao, X., Mao, X., & Li, Z. (2020). UV-shielding alginate films crosslinked with Fe^{3+} containing EDTA. *Carbohydrate Polymers, 239*, Article 115480. https://doi.org/10.1016/j.carbpol.2019.115480

Bandeira, M., Giovanela, M., Roesch-Ely, M., Devine, D. M., & da Silva Crespo, J. (2020). Green synthesis of zinc oxide nanoparticles: A review of the synthesis methodology and mechanism of formation. *Sustainable Chemistry and Pharmacy, 15*, Article 100223. https://doi.org/10.1016/j.scp.2020.100223

Belović, M., Mastilović, J. S., & Kevrešan, Ž. S. (2014). Change of surface colour parameters during storage of paprika (*Capsicum annuum* L.). *Food and Feed Research, 41*, 85–92. https://doi.org/10.5937/FFR1402085B

Cao, L., Lu, W., Mata, A., Nishinari, K., & Fang, Y. (2020). Egg-box model-based gelation of alginate and pectin: A review. *Carbohydrate Polymers, 242*, Article 116389. https://doi.org/10.1016/j.carbpol.2020.116389

Choi, I., Lee, Y., Lyu, J. S., Lee, J. S., & Han, J. (2022). Characterization of ionically crosslinked alginate films: Effect of different anion-based metal ions on the improvement of water resistant properties. *Food Hydrocolloids, 131*, Article 107785. https://doi.org/10.1016/j.foodhyd.2022.107785

Costa, M. J., Marques, A. M., Pastrana, L. M., Teixeira, J. A., Sillankorva, S. M., & Cerqueira, M. A. (2018). Physicochemical properties of alginate-based films: Effect of ionic crosslinking and mannuronic and guluronic acid ratio. *Food Hydrocolloids, 81*, 442–448. https://doi.org/10.1016/j.foodhyd.2018.03.014

Czyżowska, A., & Barbasz, A. (2022). A review: zinc oxide nanoparticles – friends or enemies? *International Journal of Environmental Health Research, 32*, 885–901. https://doi.org/10.1080/09603123.2020.1805415

da Silva, B. L., Caetano, B. L., Chiari-Andréo, B. G., Pietro, R. C. L. R., & Chiavacci, L. A. (2019). Increased antibacterial activity of ZnO nanoparticles: Influence of size and surface modification. *Colloids and Surfaces B Biointerfaces, 177*, 440–447. https://doi.org/10.1016/j.colsurfb.2019.02.013

Dash, K. K., Ali, A. N., Das, D., & Mohanta, D. (2019). Thorough evaluation of sweet potato starch and lemon-waste pectin based-edible films with nano-titania inclusions for food packaging applications. *International Journal of Biological Macromolecules, 139*, 449–458. https://doi.org/10.1016/j.ijbiomac.2019.07.193

Dojcinovic, M. P., Vasiljevic, Z. Z., Kovac, J., Tadic, N. B., & Nikolic, M. V. (2021). Nickel manganite-sodium alginate nano-biocomposite for temperature sensing. *Chemosensors, 9*, 241. https://doi.org/10.3390/chemosensors9090241

Fiordaliso, F., Bigini, P., Salmana, M., & Diomede, L. (2022). Toxicological impact of titanium dioxide nanoparticles and food-grade titanium-dioxide (E171) on human and environmental health. *Environmental Science: Nano, 9*, 1199. https://doi.org/10.1039/d1en00833a

Giz, A. S., Berberoglu, M., Beuer, S., Aydelik-Ayazoglu, S., Bayraktar, H., Alaca, B. E., & Catagil-Giz, H. (2020). A detailed investigation of the effect of calcium crosslinking and glycerol plasticizing on the physical properties of alginate films. *International Journal of Biological Macromolecules, 148*, 49–55. https://doi.org/10.1016/j.ijbiomac.2020.01.103

Gudkov, S. V., Burmistrov, D. E., Serov, D. A., Rebezov, M. B., Semenova, A. A., & Lisitsyn, A. B. (2021). A mini review of antibacterial properties of ZnO nanoparticles. *Frontiers in Physics, 9*, Article 641481. https://doi.org/10.3389/fphy.2021.641481

Han, H. Y., Yang, M. J., Yoon, C., Lee, G. H., Kim, D. W., Kwak, M., Heo, M. B., et al. (2021). Toxicity of orally administered food-grade titanium dioxide nanoparticles. *Journal of Applied Toxicology, 41*, 1127–1147. https://doi.org/10.1002/jat.4099

Jeevandanam, J., Kiew, S. F., Boakye-Ansal, S., Yon, L. S., Barhoum, A., Dauquah, M. K., & Rodrigues, J. (2022). Green approaches for the synthesis of metal and metal oxide nanoparticles using microbial and plant extracts. *Nanoscale, 14*, 2534–2571. https://doi.org/10.1039/d1nr08144f

Klaus, A., Kozarski, M., Vunduk, J., Todorovic, N., Jakovljevic, D., Zizak, Z., Pavlovic, V., Levic, S., Niksic, M., & Van Griensven, L. J. L. D. (2015). Biological potential of extracts of the wild edible basidiomycete mushroom *Grifola frondosa*. *Food Research International, 67*, 272–283. https://doi.org/10.1016/j.foodres.2014.11.035

Lau, K. Q., Sabran, M. R., & Shafie, S. R. (2021). Utilization of vegetable and fruit by-products as functional ingredient and food. *Frontiers in Nutrition, 8*. https://doi.org/10.3389/fnut.2021.661693

Lopusiewicz, L., Macieja, Sliwinski, M., Bartkowiak, A., & Roy, S. (2022). Alginate bifunctional films modified with melanin from watermelon seeds and zinc oxide/silver nanoparticles. *Materials, 15*, 2381. https://doi.org/10.3390/ma15072381

Luque, P. A., Soto-Robles, C. A., Nava, O., Gomez-Gutierrez, C. M., Castro-Beltran, A., Garrafa-Galvez, H. E., Vilchus-Nestor, A. R., & Olivas, A. (2018). Green synthesis of zinc oxide nanoparticles using *Citrus sinensis* extract. *Journal of Materials Science: Materials in Electronics, 29*, 9704–9770. https://doi.org/10.1007/s10854-018-9015-2

Mallakpour, S., Sirous, F., & Hussain, C. M. (2021). A journey to the world of fascinating ZnO nanocomposites made of chitosan, starch, cellulose and other biopolymers: Progress in recent achievements in eco-friendly food packaging, biomedical and

water remediation technologies. *International Journal of Biological Macromolecules, 170*, 701–716. https://doi.org/10.1016/j.ijbiomac.2020.12.163

Motelica, L., Ficai, D., Oprea, O., Ficai, A., Trusca, R. D., Andronescu, E., & Holban, A. M. (2021). Biodegradable alginate films with ZnO nanoparticles and citronella essential oil – a novel antimicrobial structure. *Pharmaceutics, 13*, 1020. https://doi.org/10.3390/pharmaceutics13071020

Nava, O. J., Soto-Robles, C. A., Gómez-Gutiérrez, C. M., Vilchis-Nestor, A. R., Castro-Beltrán, A., Olivas, A., & Luque, P. A. (2017). Fruit peel extract mediated green synthesis of zinc oxide nanoparticles. *Journal of Molecular Structure, 1147*, 1–6. https://doi.org/10.1016/j.molstruc.2017.06.078

Nikolic, M. V., Vasiljevic, Z. Z., Auger, S., & Vidic, J. (2021). Metal oxide nanoparticles for safe active and intelligent food packaging. *Trends in Food Science and Technology, 116*, 655–668. https://doi.org/10.1016/j.tifs.2021.08.019

Omerović, N., Djisalov, M., Živojević, K., Mladenović, M., Vunduk, J., Milenković, I., Knežević, N.Ž., Gadjanski, I., & Vidić, J. (2021). Antimicrobial nanoparticles and biodegradable polymer composites for active food packaging applications. *Comprehensive Reviews in Food Science and Food Safety, 20*(3), 2428–2454. https://doi.org/10.1111/1541-4337.12727

Omran, B. A., Aboelazayem, D., Nassar, H. N., El-Salamony, & El-Gendy, N. Sh (2021). Biovalorization of mandarin waste peels into solver nanoparticles and activated carbon. *International Journal of Environmental Science and Technology, 18*, 1119–1134. https://doi.org/10.1007/s13762-020-02873-z

Parreidt, T. S., Müller, K., & Schmid, M. (2018). Alginate-based edible films and coatings for food packaging applications. *Foods, 7*, 70. https://doi.org/10.3390/foods7100170

Paulsen, E., Barrios, S., & Lema, P. (2021). Production of packaged ready-to-eat whole strawberries (cv. San Andreas): Packaging conditions for shelf-life extension. *Food Packaging & Shelf Life, 29*, Article 100696. https://doi.org/10.1016/j.fpsl.2021.100696

Pei, X., Jiang, H., Xu, G., Li, C., Li, D., & Tang, S. (2022). Lethality of zinc oxide nanoparticles surpasses conventional zinc oxide via oxidative stress, mitochondrial damage and calcium overload: a comparative hepatoxocity study. *International Journal of Molecular Sciences, 23*, 6724. https://doi.org/10.3390/ijm23126724

Phothisarattana, D., Wongphan, P., Promhwad, K., Promsoru, J., & Harnkarnujant, N. (2022). Blown film extrusion of PBAT/TPS/ZnO nanocomposites for shelf life extension of meat packaging. *Colloids and Surfaces B, 214*, Article 112472. https://doi.org/10.1016/j.colsurfb.2021.11272

Quadrado, R. F. N., & Fajardo, A. R. (2017). Fast decolorization of azo methyl orange via heterogeneous Fenton and Fenton-like reactions using alginate-Fe^{2+}/Fe^{3+} films as catalysts. *Carbohydrate Polymers, 177*, 4430450. https://doi.org/10.1016/j.carbpol.2017.08.083

Ramezani, M., Davoodi, A., Malekizad, A., & Hosseinpour-Mashkani, A. M. (2015). Synthesis and characterization of Fe_2TiO_5 nanoparticles through a sol-gel method and its photocatalyst applications. *Journal of Materials Science: Materials in Electronics, 26*, 3957–3962. https://doi.org/10,1007/s10854-015-2930-6.

Rizzotto, F., Vasiljevic, Z. Z., Stanojevic, G., Dojcinovic, M. P., Jankovic-Castvan, I., Vujancevic, J. D., Tadic, N. B., Brankovic, G. O., Magniez, A., Vidic, J., & Nikolic, M. V. (2022). Antioxidant and cell-friendly Fe_2TiO_5 nanoparticles for food packaging application. *Food Chemistry, 390*, Article 133198. https://doi.org/10.1016/j.foodchem.2022.133198

Rodríguez-Ibarra, C., Medina-Reyes, E. I., Déciga-Alcaraz, A., Delgado-Buenrostro, et al. (2022). Food grade titanium dioxide accumulation leads to cellular alterations in colon cells after removal of a 24 h exposure. *Toxicology, 478*, Article 153280. https://doi.org/10.1016/j.tox.153280

Roger, S., Talbot, D., & Bee, A. (2006). Preparation and effect of Ca^{2+} on water solubility, particle release and swelling properties of magnetic alginate films. *Journal of Magnetism and Magnetic Materials, 305*, 221–227. https://doi.org/10.1016/j.jmmm.2006.01.005

Salama, H. E., & Abdel Aziz, M. S. (2023). Non-toxic chitosan-pyrazole adsorbent enriched with greenly synthesized zinc oxide nanoparticles for dye removal from wastewater treatment. *International Journal of Biological Macromolecules, 241*, Article 124632. https://doi.org/10.1016/j.ijbiomac.2023.124632

Salevic, A., Stojanovic, D., Levic, S., Pantic, M., Djordjevic, V., Pesic, R., Bugarski, B., Pavlovic, V., Uskokovic, P., & Nedovic, V. (2022). The structuring of Sage (*Salvia officialis L.*) extract – incorporating edible zein-based materials with antioxidant and antibacterial functionality by solvent casting versus electrospinning. *Foods, 11*, 390. https://doi.org/10.3390/foods11030390

Sani, I. K., Masoudpour-Behabadi, M., Sani, M. A., Motalebinejad, H., Juma, A. S. M., Asdagh, A., Eghabaljoo, H., Khodaei, S. M., Rhim, J. W., & Mohammadi, F. (2023). Value-added utilization of fruit and vegetable processing by-products for the manufacture of biodegradable food packaging films. *Food Chemistry, 405*, Article 134964. https://doi.org/10.1016/j.foodchem.2022.134964

Sarvanakumar, K., Sathiyaseelan, A., Mariadoss, A. V., Xiaowen, H., & Wang, M. H. (2020). Physical and bioactivities of biopolymer films incorporated with cellulose sodium alginate and copper oxide nanoparticles for food packaging application. *International Journal of Biological Macromolecules, 153*, 207–214. https://doi.org/10.1016/j.ijbiomac.2020.02.250

Sattayapanich, K., Chaiwat, W., Boonmarte, S., Bureekaem, S., & Sutthasupa, S. (2022). Alginate-based hydrogels embedded with ZnO nanoparticles as highly responsive colorimetric oxygen indicators. *New Journal of Chemistry, 46*, 19322. https://doi.org/10.1039/d2nj64164b

Shankar, S., Kasapis, S., & Rhim, J. W. (2018). Alginate-based nanocomposite films reinforced with halloysite nanotubes functionalized by alkali treatment and zinc oxide nanoparticles. *International Journal of Biological Macromolecules, 118*, 1824–1832. https://doi.org/10.1016/j.ijbiomac.2018.07.026

Shankar, S., & Rhim, J. W. (2019). Effects of types of zinc oxide nanoparticles on structural, mechanical and antibacterial properties of poly(lactide)/poly(butylene adipate-co-teraphtalate) composite films. *Food Packaging and Shelf Life, 21*(2019)), Article 100327. https://doi.org/10.1016/j.fpsl.2019.100327

Singh, J., Dutta, T., Kim, K. H., Rawat, M., Samddar, P., & Kumar, P. (2018). Green' synthesis of metals and their oxide nanoparticles: Applications for environmental remediation. *Journal of Nanobiotechnology, 16*, 84. https://doi.org/10.1186/s12951-018-0408-4

Slavin, Y. N., Asnis, J., Häfeli, U. O., & Bach, H. (2017). Metal nanoparticles: understanding the mechanisms behind antibacterial activity. *Journal of Nanobiotechnology, 15*, 65. https://doi.org/10.1186/s12951-017-0308-z

Stankic, S., Suman, S., Haque, F., & Vidic, J. (2016). Pure and multi metal oxide nanoparticles: Synthesis, antibacterial and cytotoxic properties. *Journal of Nanobiotechnology, 14*(1), 1–20. https://doi.org/10.1186/s12951-016-0225-6

Staroń, A., & Długosz, O. (2021). Antimicrobial properties of nanoparticles in the context of advantages and potential risks of their use. *Journal of Environmental Science and Health, 56*, 680–693. https://doi.org/10.1080/10934529.2021.1917936

Talebi, R., Khademolhosein, S., & Abedini, A. (2016). Synthesis and characterization of the iron titanate nanoparticles via a green method and its photocatalyst application. *Journal of Materials Science: Materials in Electronics, 27*, 2944–2949. https://doi.org/10.1007/s10854-0154114-9

Teng, K., An, Q., Chen, Y., Zhang, Y., & Zhao, Y. (2021). Recent development of alginate-based materials and their versatile functions in biomedicine, flexible electronics and environmental uses. *ACS Biomaterials Science & Engineering, 7*, 1302–1337. https://doi.org/10.1021/acs.biomaterials.1c00116

Thi, T. U. D., Nguyen, T. T., Thi, Y. D., Thi, K. H. T., Phan, B. T., & Pham, K. N. (2020). Green synthesis of ZnO nanoparticles using orange peel extract for antibacterial activities. *RSC Advances, 10*, 23899–23907. https://doi.org/10.1039/d0ra04926c

Vasiljevic, Z. Z., Dojcinovic, M. P., Vujancevic, J. D., Jankovic-Castvan, I., Ognjanovic, M., Tadic, N. B., Stojadinovic, S., Brankovic, G. O., & Nikolic, M. V. (2020). Photocatalytic degradation of methylene blue under natural sunlight using iron titanate nanoparticles prepared by a modified sol-gel method. *Royal Society of Open Science, 7*, Article 200708. https://doi.org/10.1098/rsos.200708

Vasiljevic, Z. Z., Dojcinovic, M. P., Vujancevic, J. D., Spreitzer, M., Kovac, J., Bartolic, D., Markovic, S., Jankovic-Castvan, I., Tadic, N. B., & Nikolic, M. V. (2021). Exploring the impact of calcination parameters on the crystal structure, morphology and optical properties of electrospun Fe_2TiO_5 nanofibers. *RSC Advances, 11*, 32358. https://doi.org/10.1039/d1ra05748k

Verma, R., Pathak, S., Srivastava, A. K., Prawer, S., & Tomljenovic-Hanic, S. (2021). ZnO nanomaterials: Green synthesis, toxicity evaluation and new insights in biomedical applications. *Journal of Alloys and Compounds, 876*, Article 160175. https://doi.org/10.1016/j.jallcom.2021.160175

Vizzini, P., Beltrame, E., Zanet, V., Vidic, J., & Manzano, M. (2020). Development and Evaluation of qPCR detection method and Zn-MgO/Alginate active packaging for controlling Listeria monocytogenes contamination in cold-smoked salmon. *Foods, 9*, 1353. https://doi.org/10.3390/foods9101353

Wang, H., Wan, Y., Wang, W., Li, W., & Zhu, J. (2018). Effect of calcium ions on the III steps of self-assembly of SA investigated with atomic force microscopy. *International Journal of Food Properties, 21*, 1995–2006. https://doi.org/10.10180/10942912.2018.194200

Wang, T., Wang, J., Wang, R., Yuan, P., Fan, Z., & Yang, S. (2019). Preparation and properties of ZnO/sodium alginate bi-layered hydrogel films as novel wound dressings. *New Journal of Chemistry, 43*, 8684. https://doi.org/10.1039/c9nj00402e

Yuliarto, B., Septiani, N. L. W., Kaneti, Y. V., Iqbal, M., Gumilar, G., Kim, M., Na, J., Wu, K. C. W., & Yamauchi, Y. (2019). Green synthesis of metal oxide nanostructures using natural occurring compounds for energy, environmental and bio-related applications. *New Journal of Chemistry, 43*, 15846–15856. https://doi.org/10.1039/c9nj03311d

Zanet, V., Vidic, J., Auger, S., Vizzini, P., Lippe, G., Iacumin, L., Comi, G., & Manzano, M. (2019). Activity evaluation of pure and doped zinc oxide nanoparticles against bacterial pathogens and *Saccharomyces cerevisiae*. *Journal of Applied Microbiology, 127*(5), 1391–1402. https://doi.org/10.1111/jam.14407

Zare, M., Namratha, K., Ilyas, S., Sultana, A., Hezam, A., Sunil, L., Surmeneva, M. A., Surmenev, R. S., Nayan, M. B., Ramakrishna, S., Mathur, S., & Byrappa, K. (2022). Emerging trends for ZnO nanoparticles and their applications in food packaging. *ACS Food Science and Technology, 2*, 763–781. https://doi.org/10.1021/acs.foodscitech.2c00043

Zhao, J., Wang, Y., & Liu, C. (2022). Film transparency and opacity measurements. *Food Analytical Methods, 15*, 2840–2846. https://doi.org/10.1007/s12161-022-02343-x